Emplacement of Cretaceous-Tertiary Boundary Shocked Quartz from Chicxulub Crater

Walter Alvarez,* Philippe Claeys,† Susan W. Kieffer

Observations on shocked quartz in Cretaceous-Tertiary (K-T) boundary sediments compellingly tied to Chicxulub crater raise three problems. First, in North America shocked quartz occurs above the main K-T ejecta layer. Second, shocked quartz is more abundant west than east of Chicxulub. Third, shocked quartz reached distances requiring initial velocities up to 8 kilometers per second, corresponding to shock pressures that would produce melt, not the moderate-pressure shock lamellae observed. Shock devolatilization and the expansion of carbon dioxide and water from impacted wet carbonate, producing a warm, accelerating fireball after the initial hot fireball of silicate vapor, may explain all three problems.

In wells and outcrops of uninterrupted marine sedimentary rocks outside of North America, the K-T boundary is marked by a single 1- to 10-mm clay layer often containing anomalous iridium and altered impact spherules, widely interpreted as evidence for the impact of a large comet or asteroid (*1*) at the time of the K-T mass extinction of organisms 65 million years ago (Ma). A more complicated K-T boundary stratigraphy occurs in nonmarine sediments from New Mexico, United States, to Alberta, Canada, where the boundary interval begins with a bed of kaolinitic clay, which sometimes containes goyazite spherules and is typically about 1 cm thick, overlain by a layer 1 mm to a few millimeters thick that is rich in shocked mineral grains, particularly quartz (*2*, *3*). The kaolinitic clay and goyazite spherules are probably alteration products of glassy ejecta (*4*–*6*) like that still preserved in a few sites around the Gulf of Mexico (*5*, *7*, *8*). Shocked quartz is formed under dynamic pressures of a few tens of gigapascals, depending on the target composition. An iridium anomaly is found in samples taken from the shocked quartz layer (*9*) and is attributed to the vaporization of the impacting meteorite because of pressures of many hundreds of gigapascals caused by a high-velocity impact. Some authors refer to the lower and upper layers, respectively, as the "melt-ejecta" and "fireball" layers (*10*).

Recognition of the Chicxulub structure (*11*) in the Yucatán subsurface as a giant impact crater (*12*) dating precisely from the K-T boundary at 65.0 Ma (*13*) and surrounded out to ~4000-km radius by proximal ejecta at the biostratigraphic K-T boundary (*5*, *7*, *8*) has strongly confirmed the general validity of the impact theory for the K-T mass extinction. Problems of detail remain, however, including three problems concerning the shocked quartz grains: (i) their vertical distribution in the double K-T layer of North America and their admixture with the iridium, (ii) the asymmetry of their geographic distribution about the Chicxulub crater, and (iii) their occurrence at great distances from the crater.

In North America, shocked quartz grains are virtually absent from the kaolinitic clay layer, except where apparently carried downward by biogenic disturbance. The clay layer and the quartz-bearing layer are sharply separated, and carbonized remnants of vegetation in the lower layer seem not to be present in the overlying quartz layer. This observation previously led to the notion that the layers were produced by two impact events at least one growing season apart; the vegetation traces in the lower layer were interpreted as roots of plants that grew before the overlying layer of ejecta was deposited (*14*). The lower layer was attributed to the Chicxulub impact and the upper layer to Manson crater in Iowa (*14*) until the following isotopic and age evidence eliminated Manson as a K-T candidate crater: (i) Sr, O, and Nd isotopic measurements showed the K-T impact glass to be indistinguishable from Chicxulub melt rocks but very different from Manson melt rocks (*15*). (ii) The Manson impact was dated as being earlier than the K-T boundary, at 73.8 ± 0.3 Ma (*16*). (iii) Shocked zircons from the shocked quartz layer have crystallization ages much younger than the basement rock at Manson but compatible with the granitic Pan African basement thought to characterize the Chicxulub target rock and with the crystallization age of zircons from Chicxulub melt rock (*17*). It now seems clear that both layers were produced by the Chicxulub impact and that the shocked quartz and other minerals originated from the basement granite. Iridium and quartz are believed to come from different sources: vaporized meteorite and unmelted basement rock, respectively. Problem 1 is thus, how did the shocked quartz and the iridium end up together in a separate layer, above the layer of kaolinitic clay?

The geographic distribution of K-T shocked quartz is not fully known, but it appears to be much more abundant and slightly coarser grained at longitudes west of Chicxulub. Many sites in the western interior of North America are rich in coarse shocked quartz grains (up to 0.64 mm) (*2*–*5*). In addition, shocked quartz grains are abundant and fairly coarse in all seven drill holes on the Pacific plate in which the K-T boundary has been found (*18*, *19*). This presents a sharp contrast with sites in Europe, Africa, and Asia, where shocked quartz has been difficult to find (*3*, *4*, *5*, *20*). Problem 2 is thus, why is there an asymmetry in the abundance of shocked quartz?

K-T shocked quartz grains are found as far as 10,000 km from Chicxulub crater, at Ocean Drilling Project site 596 in the southwest Pacific (*18*, *19*). Ballistic transport from Chicxulub to sites in the southwest Pacific requires a launch velocity of 7 to 8 km/s, corresponding to shock pressures that would anneal or melt the quartz, destroying the deformation lamellae that provide the evidence for shock (*21*). Problem 3 is thus, how did these shocked quartz grains achieve the velocities needed to reach distal sites without melting?

As shown below, the first two problems can be resolved if the shocked quartz traveled on steep, high-velocity ballistic trajectories. However, this requirement cannot be easily satisfied within the known constraints of impact cratering in dry silicate rocks: shocked quartz features are produced at pressures of a few tens of gigapascals, and the particle velocities obtained are less than 4 km/s on release from these pressures. Particle velocities of 7 to 8 km/s correspond to shock pressures of 50 to 100 GPa, and the product is melt, not moderately shocked quartz grains. To explain this contradiction, we propose that expansion of CO_2 and H_2O vapor released from volatile target rocks would accelerate the quartz grains from sub-

W. Alvarez and P. Claeys are in the Department of Geology and Geophysics, University of California, Berkeley, CA 94720–4767, USA, and Osservatorio Geologico di Coldigioco, 62020 Frontale di Apiro (MC), Italy. S. W. Kieffer is in the Department of Geological Sciences, University of British Columbia, Vancouver, BC V6T 1Z4, Canada.

*To whom correspondence should be addressed.
†Present address: Institut für Mineralogie, Museum für Naturkunde der Humboldt-Universität zu Berlin, Invalidenstraße 43, D-10115 Berlin, Germany.

jacent moderately shocked granite to high velocity. This process provides a mechanism to address all three problems described.

The present study is relevant not only to the specific case of the K-T boundary but also to the understanding of impact processes in general. Large impact craters are common on rocky bodies in the solar system with the exception of Earth, where craters are relatively rare because they are erased by rapid geological processes. Comparison of lunar, martian, and venusian crater morphologies, as well as field and theoretical studies of terrestrial craters (*22*) suggest that volatiles in the target body may significantly influence the impact processes and products. The Chicxulub crater is buried, so it is inaccessible but uncommonly well preserved. Study of this large, young terrestrial crater will help clarify the processes involved in comet and asteroid impact. Moreover, this was an unusual impact because of the combined carbonate and granite target lithologies, which would have generated large amounts of CO_2 and H_2O. Kieffer and Simonds (*22*) and O'Keefe and Ahrens (*23*) have given general consideration to the role of CO_2 and H_2O vapor in impact and the impact cratering process; we now apply these considerations to the specific case of the Chicxulub crater.

Global-Scale Ballistics of the Ejecta

We suggest that both the distribution of the shocked quartz and its occurrence in a separate layer can be explained by transport of the quartz grains on ballistic trajectories different from those of the glassy ejecta which altered to form the kaolinitic clay layer. We have calculated the reimpact loci of ballistic ejecta from Chicxulub as a function of the velocity and elevation angle of launch, taken around a 360° range of launch azimuths (*24*). Except when interacting with the atmosphere during launch and re-entry, ballistic ejecta particles follow elliptical orbits with one focus at Earth's center, when plotted in inertial coordinates, until they reimpact Earth's surface. We ignore atmospheric interactions during re-entry, considering them to have only a minor effect on the deposition point of sand-sized grains. However, settling times through the atmosphere may complicate our conclusions and need further consideration when more data on particle size and atmospheric conditions after impact are available. Interactions during launch are important and are discussed below, but the size of the expanding ball of gas around the impact site is small compared with long-range trajectories, so the particles can be treated as if launched into ballistic trajectories from the impact site once they leave the atmosphere.

Earth's rotation has two interesting effects on these orbits. The first effect is that the semimajor axis of the elliptical orbit depends only on the launch velocity in the inertial reference frame (*25*); to find this velocity, the eastward rotational velocity of Earth (0.463 km/s at the equator) is added to the target-frame launch velocity of eastbound particles, but subtracted from that of westbound particles. This has little effect on the semimajor axis of slow particles, but at launch velocities from about 8 or 9 km/s up to escape velocity (11.2 km/s), eastbound particles go higher and stay up longer than the corresponding westbound ones. The second effect is that, because Earth rotates beneath in-flight ejecta, the reimpact site is at the same latitude but displaced to the west, as compared with a nonrotating Earth. This effect is small for slow ejecta, but important for fast ejecta.

Because of these effects, there is a forbidden zone east of the impact site that cannot be reached by eastbound ejecta unless the launch velocity is high and the elevation angle low (Fig. 1). All of Europe and Africa is in the forbidden zone for ejecta launched at 70°, and all except the extreme western margin is forbidden at 60°. At 50°, the forbidden zone is reduced to a small area around India and eastern Africa. The known distribution of K-T shocked quartz would be well explained if most shocked quartz grains were launched from Chicxulub on trajectories steeper than about 65°.

Developing this concept, we propose that the double layer of ejecta in the western interior of North America reflects two different launch mechanisms during the cratering event. It has been proposed that the clay in the lower layer was formed by the alteration of glassy ejecta launched as part of the ejecta curtain (*4–6*). The ejecta curtain observed in hypervelocity impact experiments is an outward-expanding, downward-pointing cone inclined ~45° to the horizontal (*26*) and represents the coherent front of solid and melt ejecta particles on independent trajectories, launched at elevation angles ≤45° [figure 17 in (*27*); figure 6.4 in (*28*)]. Because a 45° elevation angle yields the longest ballistic range for a given launch velocity, this material will be the first to arrive at a given site (Fig. 2). For example, to reach the K-T site at Clear Creek, Colorado, ballistic ejecta launched from Chicxulub at an angle of 45° above the horizon requires an initial velocity of 4.4 km/s and has a travel time of 14 min. In contrast, if the shocked quartz at Clear Creek was launched at an elevation angle of 70°, as suggested by the global distribution, its initial velocity was 5.7 km/s and its travel time was 28 min. Ejecta-curtain particles launched at 30° to 45° have travel times to Clear Creek of about 10 to 15 min, whereas steeper ejecta particles, launched at

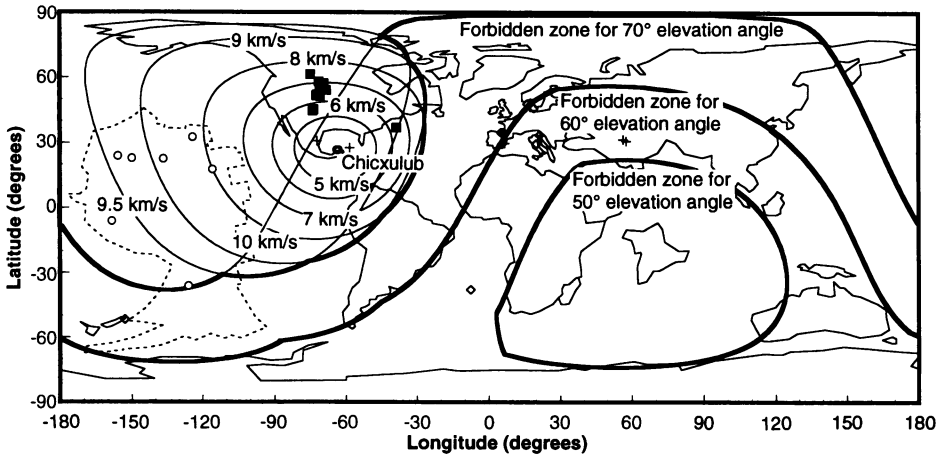

Fig. 1. Reimpact patterns of ballistic ejecta launched at Chicxulub shown on a map of continental positions at K-T boundary time (the dashed line bounds pre–K-T Pacific plate that has not subsequently been subducted) (*35*). These patterns ignore atmospheric effects, which occur only at the times of launch and re-entry. For a launch angle of 70° above the horizon, thin lines show reimpact loci for launch velocities at 1-km/s increments. Heavy lines show the limit of the forbidden zone at 70° as well as for 60° and 50° launch angles; in the latter two cases reimpact loci are omitted to avoid clutter (*36*). Solid squares mark sites with coarse shocked quartz (grains >250 μm in diameter); circles mark sites with abundant fine shocked quartz; diamonds mark sites with rare, fine shocked quartz; and crosses mark sites where shocked quartz has been reported, but information is insufficient to determine its abundance. Schultz has suggested that the abundance of shocked quartz in the U.S. western interior K-T sites reflects a low-angle oblique impact toward the northwest (*37*). Alternatively, we propose that the asymmetrical distribution of shocked quartz grains, heavily concentrated west of the impact site, can be explained if most grains were launched at an angle steeper than ~65°.

65° to 80°, have travel times of 23 to 63 min. Thus, all the ejecta-curtain material would have arrived at Clear Creek before any of the steep ejecta began to fall (Fig. 2). For a more northern site, like Brownie Butte, Montana, the corresponding travel times are 13 to 18 min for ejecta curtain particles and >33 min for steep ejecta.

This travel time sorting may explain the double layer of the western interior, but not if the organic traces in the lower layer represent the roots of plants that grew between two falls, which would thus be separated by at least one growing season. We suggest instead that the organic traces may mark the stems of plants that burned during the arrival of the particles of the lower layer, heated by their atmospheric re-entry (*28, 29*), and that had fully burned (*30*) and collapsed before the fall of the second layer.

Model of the Cratering Event

A cratering model is required that explains the high velocities, near-vertical trajectories, and relatively cool temperatures needed for the shocked quartz to be carried far to the west and not annealed. To examine the cratering process, we used the semianalytic model of Kieffer and Simonds (*22*), in which the processes that occur during an impact event are subdivided into seven successive, sometimes overlapping, stages: stage 1, initial contact; stage 2, compression and release of the meteorite; stage 3, rarefaction and attenuation in the target; stage 4, excavation and flow within the crater; stage 5, ejecta launch and fallback; stage 6, mechanical modification; and stage 7, hydrothermal and chemical alteration.

In this article, we consider primarily stages 2 through 5. For each stage, the appropriate conservation laws and thermodynamic properties (or approximations) were solved to yield properties such as depth of penetration, duration of each stage, peak shock pressure in the meteorite and ground, and attenuation of peak pressure as a function of distance from the meteorite at its point of maximum penetration. Although this model is simplistic when compared with computer simulations such as those of O'Keefe and Ahrens (*23*) and Roddy *et al.* and Vickery and Melosh (*30*), it has the advantage of providing a relatively intuitive overview of the whole cratering process. The results (*31*) are in reasonable semiquantitative agreement with these earlier models and are in particularly good agreement with the model of Pope *et al.* (*32*) who did a similar calculation based on anhydrite thermodynamics in order to estimate climate effects. The sensitivity of the model to impact velocity and to meteorite and target composition is discussed in detail by Kieffer and Simonds (*22*).

We assume that a stony meteorite 10 km in diameter traveling at 24.6 km/s strikes a region with a 3-km-thick layer of wet carbonate overlying a granitic basement (*33*). During stage 2 and the early parts of stages 3 and 4, the shock Hugoniots and high-pressure parts of the release adiabats are relatively independent of rock type, and for these stages the shock equation-of-state properties used are those of diabase for the stony meteorite and those of granite for the target rock. The properties of volatile rocks become important later in the cratering event and are considered separately below. The meteorite is assumed to have a density of 3000 kg/m^3, with a corresponding mass of 1.6×10^{15} kg and kinetic energy of 4.8×10^{23} joules (114×10^6 Mton).

On contact (stage 1), a shock wave is propagated into the target at nearly 20 km/s, shocking both the meteorite and the target up to a pressure of 660 GPa (Fig. 3A). For the first 0.5 s (stage 2), while the shock wave travels to the back of the meteorite, the meteorite penetrates through the carbonate and into the granite. The shock wave that is simultaneously traveling into the ground accelerates material downward or radially away from the meteorite, but not yet upward.

When the shock wave reflects from the back of the meteorite, it becomes a rarefaction wave that releases the shocked meteorite, and eventually the shocked target rock, back toward ambient pressure (stage 2b and Fig. 3, B and C). By the time the rarefaction reaches the meteorite-target interface, the meteorite has reached the end of its penetration path at 13 km. The meteorite and a closely adjacent mass of rock of roughly equivalent mass are vaporized and begin ascending in a hot fireball.

Although some energy is released along the whole penetration path, and although free-surface effects on the meteorite and target rock are important in detail (*23, 32*), to first order the process can be modeled by examining the decay of the peak-pressure isobars radially from a maximum value of 660 GPa centered in a mass of material at the depth of penetration (Fig. 3, B and C). Because the depth of penetration is only about one meteorite diameter, the shock waves penetrating downward have a different decay pattern than those moving toward, and reflecting from, the surface (*22, 23, 30, 32*). This causes radial differences in peak pressure which, combined with the different lithologies along different paths, influences the state of shocked material ejected.

In dry silicate rocks, the products of shock decompression vary with pressure in

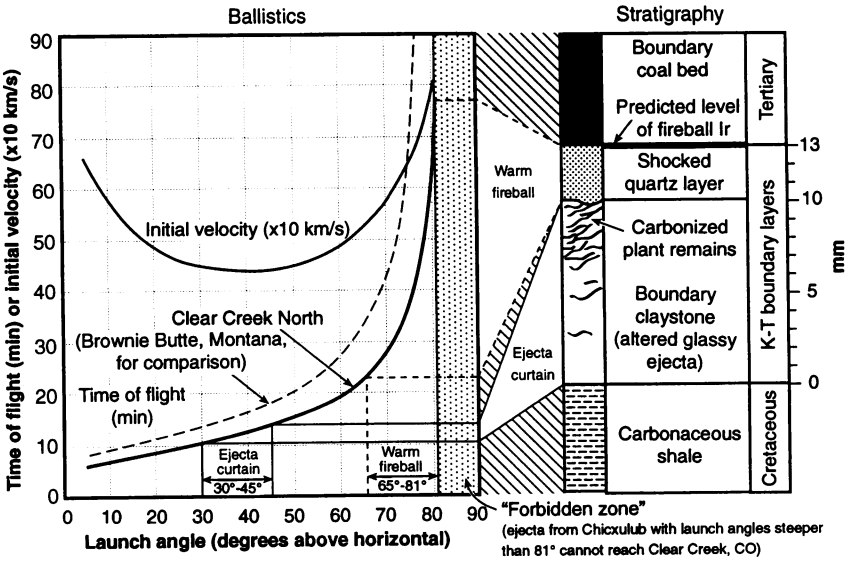

Fig. 2. Calculated history of ejecta arrival at Clear Creek, Colorado (37° 05.26′ N, 104° 31.33′ W), compared with the fine-scale stratigraphy of the K-T boundary at the Clear Creek North site of Izett (*3*), ignoring atmospheric effects during launch and re-entry. The boundary clay layer is made largely of kaolinitic clay, probably resulting from alteration of glassy ejecta (*4–6*). If launched in an ejecta curtain like that observed in experiments many orders of magnitude smaller, these particles would have had launch angles of 30° to 45° and would have reached this site in 10 to 15 min, with launch and reimpact velocities close to 4.5 km/s. The overlying layer is rich in shocked quartz. If these grains traveled on trajectories steeper than ~65°, as inferred from the geographic distribution of shocked quartz (Fig. 1), they would have had initial velocities >5.2 km/s and would have arrived >23 min after the impact. Launch velocities this high would imply energies sufficient to melt these obviously unmelted grains (*21*), so we infer that they were accelerated in an expanding "warm fireball" of CO_2 and H_2O vapor. Wispy carbonized remains within the boundary claystone, previously interpreted as the roots of plants that grew in an interval of ≥1 year between deposition of the two layers, may instead represent the stems of plants ignited by infrared heat from re-entry of the early ejecta and covered a few minutes later by the shocked quartz.

the following sequence: vaporized meteorite and vaporized rock (shocked to pressures over 100 GPa), melted rock (shocked to pressures >50 GPa roughly), highly and moderately shocked rock (including shocked quartz grains and shocked feldspars at pressures of a few tens of gigapascals), weakly shocked, and then fractured rock. These are the products that we would expect to form sequentially and temporally as the shock wave decays down and out into the granite. For example, in this model, the peak pressure of 660 GPa is attained at 13 km depth, and 15 GPa at a depth of 30 km. Thus, we expect shocked quartz to be produced under the meteorite site at depth.

A hot fireball is formed from vaporized material surrounding the penetration cavity (Fig. 3, B and C). The rise of this vapor from the impact site may be coupled with other atmospheric phenomena such as atmospheric preheating during entry of the meteorite and explosions if the meteorite had partly disintegrated within the atmosphere (*34*). Complicated shock waves travel in the air, both from the initial meteorite entry and from the rising and decompressing fireball. This hot vaporized material is rich in meteoritic components and in vaporized components from near the penetration cavity, carbonate and silicate in this case.

The strongly, moderately, and some of the weakly shocked material surrounding the impact site and lining the walls of the expanding transient cavity is turned upward and outward by rarefaction waves. This flow develops into the ejecta curtain formed by the coherent front of melt and solid ejecta launched at an angle of ≤45° and at velocities of a few kilometers per second. It would be expected that the shocked quartz produced deep under the impact point proximal to the melt zone would largely be entrained in the ejecta curtain (*22*). However, if 4.5 km/s is the maximum launch velocity that will not anneal or melt shock features (*21*), then shocked grains will travel no farther than the Gulf Coast of the United States (*24*); this agrees with the presence of rare shocked quartz in ejecta-curtain (lower layer) deposits in the Gulf of Mexico K-T sections (*8*) and the absence of shocked quartz in the lower K-T layer in the western United States (*3–5*) (Fig. 1).

In the granite above the depth of penetration we would expect the same sequence of shocked products as produced below the meteorite. The relative abundances will be different than below the meteorite because they are influenced not only by radial pressure decay but by free-surface and entry path effects. We estimate that at a radial distance of ~10 km from the center of impact, shock pressures are a few tens of gigapascals, and lamellae and other deformation features should be produced in the granite.

The wet carbonate cover, however, has a vastly different behavior in these pressure ranges. Wet carbonate can produce CO_2 and H_2O vapor at relatively low pressure; devolatilization of incorporated anhydrite would also contribute volatiles over approximately the same pressure range. Although data are sparse and somewhat inconsistent, in general it is agreed that carbonates partially break down into CaO and CO_2 on decompression from ~45 GPa and completely break down if shocked to over ~70 GPa. The pressure range for anhydrite breakdown is similar, although the degree of equilibrium attained in any of these devolatilization reactions is a subject of much controversy. In our simple model, 70 GPa is reached at a radius of ~11 km (surface) and 45 GPa at about 12 km. Water in pores and cracks will vaporize if shocked to over 10 GPa, reached at a surface radius of 18 km in this model.

Material in the carbonate layer out to a radius of at least 18 km will partially or even totally vaporize, releasing a mixture of steam, CO_2, oxides, and fragments of the carbonate. This is a very large amount of vapor. If we consider only an annulus of carbonate between 11- and 18-km radius, shocked to between 70 and 10 GPa, the volume of material is 2000 km^3. At a density of 2500 kg/m^3 (purposely reduced from the density used for average shock wave properties of the target to allow for some porosity and water content), the mass would be 5×10^{15} kg, approximately three times the mass of the impacting meteorite. A typical energy for vaporizing this material is about 10^{13} ergs/kg. If only 10% of the material vaporized, this would require input of 3×10^{27} ergs, or about 10^5 Mton. This energy would be deposited in the vapor on a time scale of a few seconds.

We suggest that the CO_2 and H_2O vapor from this devolatilized carbonate zone between ~10 and 20 km (rounded off) ascended as a "warm fireball" which dragged

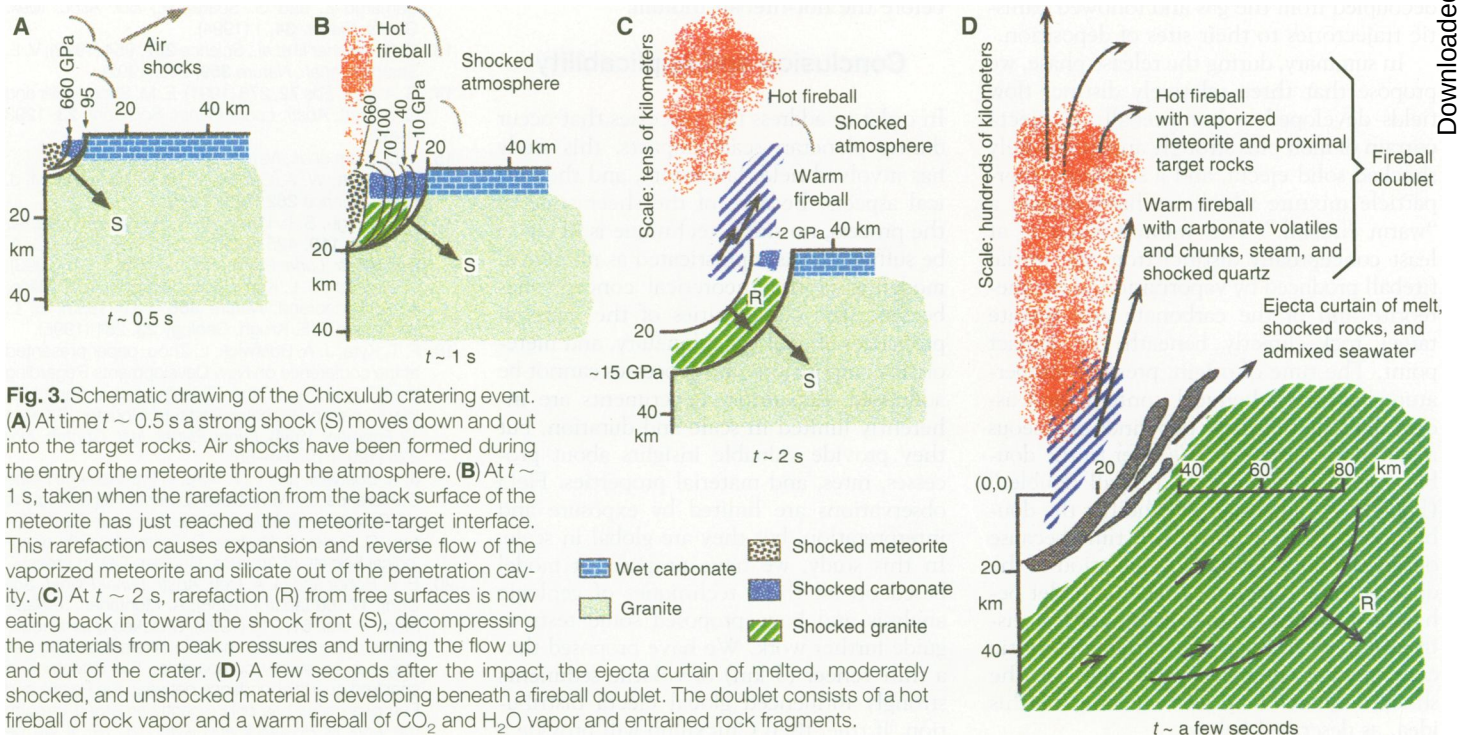

Fig. 3. Schematic drawing of the Chicxulub cratering event. (**A**) At time $t \sim 0.5$ s a strong shock (S) moves down and out into the target rocks. Air shocks have been formed during the entry of the meteorite through the atmosphere. (**B**) At $t \sim 1$ s, taken when the rarefaction from the back surface of the meteorite has just reached the meteorite-target interface. This rarefaction causes expansion and reverse flow of the vaporized meteorite and silicate out of the penetration cavity. (**C**) At $t \sim 2$ s, rarefaction (R) from free surfaces is now eating back in toward the shock front (S), decompressing the materials from peak pressures and turning the flow up and out of the crater. (**D**) A few seconds after the impact, the ejecta curtain of melted, moderately shocked, and unshocked material is developing beneath a fireball doublet. The doublet consists of a hot fireball of rock vapor and a warm fireball of CO_2 and H_2O vapor and entrained rock fragments.

with it not only shocked fragments from the carbonate from which it originated but also moderately shocked fragments from the subjacent granite near the contact. We did not attempt to estimate the velocity of this fireball with our model because by the time it formed, the atmosphere was highly altered by previous shocks, and details of cratering geometry and free surfaces have become important. Experimental data on dry and wet, nonporous and porous, media show that the maximum launch velocity obtainable from shock pressures of 30 GPa is 7 km/s, somewhat under our desired value of 8 km/s (*21*).

Buoyancy effects and atmospheric-scale pressure gradients may be equally important. Jones and Kodis (*34*) have suggested that if the energy deposited suddenly in a compressed gas exceeds ~12,000 Mton, a fireball, unconfined by the atmosphere, will rise, passing the point of neutral buoyancy where pressure and density become equal to atmospheric pressure and density, before it decompresses completely. For comparison we estimated above that the warm fireball had $\sim 10^5$ Mton of energy, more than sufficient for this unconfined buoyant rise. In this case, the fireball continues accelerating upward along the decreasing atmospheric pressure gradient. We hypothesize that the volume of shocked carbonate and aqueous gases produced in the zone peripheral to the hot fireball ascended rapidly with fireball-like buoyancy dynamics and that this warm fireball accelerated the shocked granite fragments to velocities of 8 to 11 km/s and into nearly vertical paths (Fig. 3D). As the warm fireball expanded, the solid particles decoupled from the gas and followed ballistic trajectories to their sites of deposition.

In summary, during the release phase, we propose that three relatively distinct flow fields developed: a hot fireball, an ejecta curtain of melt plus strongly and moderately shocked solid ejecta, and a separate vapor-particle mixture which we have termed a "warm fireball." The warm fireball is at least conceptually distinct from the initial fireball produced by vaporization of the meteorite and of the carbonate and silicate target rock directly beneath the impact point. The time of origin, pressure-temperature histories, chemical content, and ascent dynamics of these two kinds of gaseous material are different. We refer to the double gaseous regime as a "fireball doublet" (Fig. 3D). We cannot say whether the doublet merges or separates with time because our model does not allow calculation of the detailed time history of fireball-doublet behavior. Detailed studies of the vertical distribution of iridium and other meteoritic components compared with that of the shocked quartz may allow testing of this idea, as described below.

Prediction of a Third Layer

The K-T impact bed in the western United States contains two clearly recognizable layers. We interpret the lower layer as representing the ejecta curtain and the upper layer as derived from the warm fireball. The iridium anomaly is found in samples taken from the upper layer. The carrier for iridium has never been recognized in any K-T sites, and it probably occurs in extremely fine particles. Iridium and quartz come from different sources: vaporized meteorite and unmelted basement, respectively. The iridium is likely to have been deposited as a separate veneer on the top of this upper layer because of the slow settling of fine particles. Iridium does occur in the finest material at the top of the marine K-T boundary beds in the deep Gulf of Mexico (*8*). We therefore predict (Fig. 2) that even higher resolution iridiumstratigraphy should reveal a triple boundary layer at sites in the western United States, with the three layers related to three distinct mechanisms for launching ejecta during the impact event: (i) An extremely hot fireball consisting of vaporized meteorite and target-rock carbonate and silicate is launched first, but because of the fine grain size of the material it carries, this is the last portion to settle. (ii) A ~45° ejecta curtain carries melted and shocked solid rock fragments that are emplaced first because of their lower, more direct trajectories. (iii) A quite distinct warm fireball of CO_2 and steam accelerates moderately shocked granite fragments into ballistic trajectories steeper than about 65°, and they arrive after the ejecta curtain material but before the hot-fireball iridium.

Conclusion and Applicability

In order to address the processes that occur during planetary-scale impacts, this study has involved field, laboratory, and theoretical aspects. Because of the sheer scale of the process, no single technique is likely to be sufficient. As sophisticated as numerical modeling of the theoretical concepts has become, the complexities of the material properties of geologic, planetary, and meteoritic compositions and processes cannot be addressed. Laboratory experiments are inherently limited in scale and duration, but they provide valuable insights about processes, rates, and material properties. Field observations are limited by exposure and interpretation, but they are global in scale. In this study, we have proposed a model based on all three techniques of geologic analysis and have proposed some tests to guide further work. We have proposed that a thin veneer (3 km) of volatile sediments strongly influenced global ejecta distribution. If true, then Chicxulub will provide a valuable analog for impact studies on both dry planets (moon, Mercury) and volatile-containing planets (Mars, Venus).

REFERENCES AND NOTES

1. L. W. Alvarez, W. Alvarez, F. Asaro, H. V. Michel, *Science* **208**, 1095 (1980); J. Smit and J. Hertogen, *Nature* **285**, 198 (1980); F. T. Kyte, Z. Zhou, J. T. Wasson, *ibid.* **288**, 651 (1980); J. Smit and G. Klaver, *ibid.* **292**, 47 (1981); A. Montanari *et al.*, *Geology* **12**, 696 (1984).
2. B. F. Bohor, E. E. Foord, P. J. Modreski, D. M. Triplehorn, *Science* **224**, 867 (1984); G. A. Izett and C. L. Pillmore, *Eos* **66**, 1149 (1985); C. L. Pillmore and R. M. Flores, *Geol. Soc. Am. Spec. Pap.* **209**, 111 (1987).
3. G. A. Izett, *Geol. Soc. Am. Spec. Pap.* **249**, 1 (1990).
4. B. F. Bohor, *ibid.* **247**, 335 (1990).
5. C. Koeberl and H. Sigurdsson, *Geochim. Cosmochim. Acta* **56**, 2113 (1992).
6. B. F. Bohor, B. P. Glass, W. J. Betterton, *Abstr. Lunar Planet. Sci. Conf.* **24**, 145 (1993); R. M. Pollastro and B. F. Bohor, *Clays Clay Miner.* **41**, 7 (1993).
7. G. A. Izett, *J. Geophys. Res.* **96**, 20879 (1991); F. J.-M. R. Maurrasse and G. Sen, *Science* **252**, 1690 (1991); H. Sigurdsson *et al.*, *Nature* **349**, 482 (1991); J. Smit *et al.*, *Proc. Lunar Planet. Sci. Conf.* **22**, 87 (1992); C. Koeberl, *Geochim. Cosmochim. Acta* **56**, 4319 (1992).
8. W. Alvarez *et al.*, *Geology* **20**, 697 (1992); J. Smit *et al.*, *ibid.*, p. 99; P. Claeys, W. Alvarez, J. Smit, A. R. Hildebrand, A. Montanari, *Abstr. Lunar Planet. Sci. Conf.* **24**, 297 (1993); J. Smit, T. B. Roep, W. Alvarez, P. Claeys, A. Montanari, *Geology* **22**, 953 (1994).
9. C. J. Orth, M. Attrep Jr., L. R. Quitana, *Geol. Soc. Am. Spec. Pap.* **247**, 45 (1990).
10. A. R. Hildebrand and W. V. Boynton, paper presented at the 2nd Conference on Global Catastrophes in Earth History, Snowbird, UT, 20 to 23 October 1988, *Lunar Planet. Inst. Contrib. No. 673* (1988), p. 78; B. F. Bohor and W. J. Betterton, *Abstr. Lunar and Planet. Sci. Conf.* **21**, 107 (1990); B. F. Bohor and B. P. Glass, *Meteoritics* **30**, 182 (1995).
11. A. Cornejo T. and A. Hernandez O., *Bol. Asoc. Mex. Geol. Pet.* **2**, 453 (1950).
12. G. T. Penfield and A. Camargo Z., *Soc. Explor. Geophys. Tech. Program, Abstr. Biogr.* **51**, 37 (1981); A. R. Hildebrand *et al.*, *Geology* **19**, 867 (1991); A. Camargo Z. and G. Suárez R., *Bol. Asoc. Mex. Geof's. Explor.* **34**, 1 (1994).
13. C. C. Swisher III *et al.*, *Science* **257**, 954 (1992); V. L. Sharpton *et al.*, *Nature* **359**, 819 (1992).
14. G. A. Izett, *Eos* **72**, 278 (1991); E. M. Shoemaker and G. A. Izett, *Abstr. Lunar Planet. Sci. Conf.* **23**, 1293 (1992).
15. J. D. Blum *et al.*, *Nature* **364**, 325 (1993).
16. G. A. Izett, W. A. Cobban, J. D. Obradovich, M. J. Kunk, *Science* **262**, 729 (1993).
17. T. E. Krogh, S. L. Kamo, B. F. Bohor, *Earth Planet. Sci. Lett.* **119**, 425 (1993); W. R. Premo and G. A. Izett, *Abstr. Lunar Planet. Sci. Conf.* **24**, 1171 (1993); T. E. Krogh, S. L. Kamo, V. L. Sharpton, L. E. Marin, A. R. Hildebrand, *Nature* **366**, 731 (1993); S. L. Kamo and T. E. Krogh, *Geology* **23**, 281 (1995).
18. F. T. Kyte, J. A. Bostwick, L. Zhou, paper presented at the conference on New Developments Regarding the KT Event and Other Catastrophes in Earth History (Lunar and Planetary Institute, Houston, TX, 9 to 12 February 1994), *Lunar Planet. Inst. Contrib. No. 825* (1994), pp. 64–65.
19. J. A. Bostwick and F. T. Kyte, in *Proceedings of the Conference on New Developments Regarding the KT Boundary and Other Catastrophes in Earth History*, G. Ryder, S. Gartner, D. Fastovsky, Eds. (Geological Society of America, Boulder, CO, in press).
20. B. F. Bohor and G. A. Izett, *Abstr. Lunar Planet. Sci. Conf.* **17**, 68 (abstr.) (1986); A. Montanari, *J. Sediment. Petrol.* **61**, 315 (1990). Shocked quartz abundance determinations made in different laboratories may not be strictly comparable. The difference in shocked quartz abundance between the Pacific and European sites has only recently emerged through the work of Bostwick and Kyte (*18, 19*). It will be

important to have sites from the two areas compared in the same laboratory.
21. Deformation features are directly correlated with peak shock pressure. Numerous studies show that moderate shock features (reduced refractive index, lamellar features) form at pressures between 20 and 40 GPa (depending on the rock type), and shock-fused quartz at pressures above 50 GPa. In turn, peak shock pressure is directly related to the particle velocity attained behind the shock. To a very good approximation in dry rocks, the velocity is doubled by the passing rarefaction [R. G. McQueen, S. P. Marsh, J. N. Fritz, *J. Geophys. Res.* **72**, 4999 (1967)]. For a peak shock pressure of 20 GPa, the measured shock velocities in 12 representative rocks are 0.8 to 1.4 km/s. The rarefaction velocities are then in the range of 1.6 to 2.8 km/s. Ahrens and Rosenberg [in *Shock Metamorphism of Natural Minerals*, B. French and N. Short, Eds. (Mono, Baltimore, MD, 1968), p. 59] extended the range of pressures to 45 GPa and measured all rarefaction (free surface) velocities to be less than 4.5 km/s. We therefore take 4.5 km/s as an upper limit on the velocity that could be attained by moderately shocked quartz grains launched by a simple cratering event in dry rocks. At higher pressures, higher rarefaction velocities are obtained, but the features of moderately shocked quartz are not preserved because the quartz is annealed or fused. Target rock texture (porosity in this case) and wetness also affect shock metamorphic features and rarefaction velocities [S. W. Kieffer, *J. Geophys. Res.* **76**, 5449 (1971)]. A significant effect for this discussion is that porosity and volatile content both increase the possible rarefaction velocities. For example, dry soil (~porous quartz soil) shocked to 30 GPa releases with a velocity of ~5.7 km/s, higher than that measured for single crystal or nonporous polycrystalline quartz. Wet soil shocked to the same pressure releases with a particle velocity of ~7.3 km/s [G. D. Anderson *et al.*, *Technical Report AFWL-TR-65-146* (SRI International, Menlo Park, CA, 1966)]. Thus, an impact into porous, water-saturated carbonates will produce products with significantly higher velocities than a similar impact into a dry, nonporous silicate target.
22. S. W. Kieffer and C. H. Simonds, *Rev. Geophys. Space Phys.* **18**, 143 (1980).
23. J. D. O'Keefe and T. J. Ahrens, *Geol. Soc. Am. Spec. Pap.* **190**, 103 (1982); *Nature* **338**, 247 (1989).
24. W. Alvarez, in (*19*). The necessary equations were modified from those given by A. Dobrovolskis [*Icarus* **47**, 203 (1981)]. His dimensionless parameters were converted to Earth's case as follows: 1 time unit = 806.3 s, 1 length unit = 6371 km, and 1 mass unit = 5.973×10^{27} g. Time-of-flight calculations follow those described by A. D. Dubyago [*The Determination of Orbits* (Macmillan, New York, 1961)].
25. The semimajor axis, $a = 1/(2 - v^2)$ in dimensionless units, where v is the launch velocity.
26. P. H. Schultz and D. E. Gault, *Geol. Soc. Am. Spec. Pap.* **190**, 153 (1982).
27. V. R. Oberbeck, *Rev. Geophys. Space Phys.* **13**, 337 (1975).
28. H. J. Melosh, *Impact Cratering: A Geologic Process* (Univ. of Arizona Press, Tucson, 1988)
29. H. J. Melosh, N. M. Schneider, K. J. Zahnle, D. Latham, *Nature* **343**, 251 (1990).
30. D. J. Roddy *et al.*, *Int. J. Impact Eng.* **5**, 525 (1987); A. M. Vickery and H. J. Melosh, *Geol. Soc. Am. Spec. Pap.* **247**, 289 (1990).
31. The sensitivity of the impact cratering model to varying meteorite and target compositions and to impact velocity can be found in (*22*), especially tables 2 to 4, and figures 6 and 7. During the compression stage of an impact, peak shock pressure depends on the material properties of the meteorite and target and on the impact velocity. We ran a range of simulations for impact of a stony meteorite into targets of diabase, permafrost, carbonate, granite, and water [properties all given in (*22*)]. Peak pressures ranged from a minimum of 380 GPa (ice target) to 555 GPa (permafrost), to 657 GPa (granite), to 705 GPa (diabase). In all cases, energy was partitioned about half into the target and half into the meteorite during the compression stage. The ratio of penetration depth to meteorite radius ranged from a minimum of 2.6 (diabase, carbonate, granite) to 3.2 (permafrost), to a maximum of 4.3 (liquid water).
32. K. O. Pope, K. H. Baines, A. C. Ocampo, B. A. Ivanov, *Earth Planet. Sci. Lett.* **128** (N3-4), 719 (1994).
33. E. López Ramos, *Geol. Mex.* **3**, 277 (1981). The "rocas volcánicas" mentioned on p. 277 are probably the impact melt rocks of the Chicxulub crater, not basement rock.
34. E. M. Jones and J. W. Kodis, *Geol. Soc. Am. Spec. Pap.* **190**, 175 (1982).
35. Continental positions calculated with the 66-Ma rotation parameters of the University of Chicago Paleogeographic Atlas Project, D. Rowley, personal communication.
36. At velocities greater than 10 km/s, ejecta can travel farther west, but not farther east, so these are firm limits on the west edge of the forbidden zone for each elevation angle. Cusps in the boundaries of the forbidden zones are an artifact produced by joining segments of reimpact loci lines at 1-km/s increments.
37. P. H. Schultz, in (*18*), pp. 105–106.
38. We thank J. Bostwick and F. T. Kyte for discussion and for a preprint of their work on the K-T boundary of the Pacific plate and D. Rowley for plate-rotation parameters. Comments by R. Jeanloz and C. Koeberl on an earlier version of this manuscript are greatly appreciated. Supported by the National Aeronautics and Space Administration (NASA) grant NAGW-3008 and NSF grant EAR-91-05297 to W.A., NASA grant NAGW-1740 to S.W.K., and University of California Berkeley Esper A. Larsen Jr. Research Fund.

Resonance Light Scattering: A New Technique for Studying Chromophore Aggregation

Robert F. Pasternack and Peter J. Collings

Light scattering experiments are usually performed at wavelengths away from absorption bands, but for species that aggregate, enhancements in light scattering of several orders of magnitude can be observed at wavelengths characteristic of these species. Resonance light scattering is shown to be a sensitive and selective method for studying electronically coupled chromophore arrays. The approach is illustrated with several examples drawn from porphyrin and chlorin chemistry. The physical principles underlying resonance light scattering are discussed, and the advantages and limitations of the technique are reviewed.

We have recently reported (*1*) on a new resonance technique called resonance light scattering (RLS) that is both extremely sensitive and selective in probing chromophore aggregation in a number of different systems. The theory behind this technique is not new, and in fact RLS has been tried in the past for purposes other than studying aggregation. In those cases, the technique was only marginally successful. However, we have found that in aggregation experiments, RLS not only meets sensitivity and selectivity criteria but offers the additional benefits of simplicity and versatility. In this article, we describe the basic physics behind RLS, survey some ongoing research on its refinement and application to different systems, and discuss a number of areas in which RLS may make important contributions in the near future.

Experimental Approaches to Studying Aggregation

The recent flurry of research activity on supramolecular assemblies and their application in the construction of nanodevices has encouraged the development of experimental techniques capable of detecting and characterizing these assemblies. Understanding the chemical, biological, and pharmacological activity of a complex system requires knowledge of the state of molecular aggregation of the system's components. Research issues that involve relations between the properties of complex systems and the formation of large aggregates include (i) the organization of chlorophyll and other pigments in chlorosomes, in which a particular molecular assembly is required for efficient photosynthesis (*2*); (ii) the relation of photosensitization efficiency to the extent of aggregation of the active component at cancer cells, which must be resolved to enable rational design of alternative reagents in photodynamic cancer therapy (*3*); and (iii) the state of aggregation of lipids and drugs in liposomes, which has been shown in certain cases to be a crucial factor in their effectiveness in treating disease (*4*). Although light scattering experiments are frequently used to study such problems, in these three examples conventional light scattering would likely not yield useful data because of the background signals provided by the medium; not only the existence but the identity of the scatterer must be determined.

Even though light scattering experiments

R. F. Pasternack is in the Department of Chemistry and P. J. Collings is in the Department of Physics and Astronomy at Swarthmore College, 500 College Avenue, Swarthmore, PA 19081, USA.